CHAPTER 22

ENERGY DISSIPATION AND AIR BUBBLES MIXING INSIDE SURF ZONE

Hwung Hweng Hwung[1] Jih Ming Chyan[2] Yeong Chyang Chung[3]

Abstract

In order to understand the relationship between entrained air bubbles and energy transfer inside surf zone, a special technique of He–Ne laser and 2D LDV were employed to investigate the characteristics of air bubbles concentration and velocity fields, respectively. The experimental results shows that the concentration profiles of air bubbles decay hyperbolically in the vertical direction and exponentially in the horizontal direction. With appropriate parameter groups, the distributions of air bubbles show a characteristics of similarity. The potential energy, kinematic energy and total energy decrease with the horizontal distance except that the kinematic energy slightly increases between the impinging point and the maximum penetration. Within this region, the energy loss of potential energy and kinematic energy is almost transferred to the air bubbles to merge into the water body.

Introduction

The wave breaking in the nearshore area is a very important and fascinating phenomenon of wave hydrodynamics. In the instant of wave

[1] Professor of Hydraulic and Ocean Engineering Department, Director of Tainan Hydraulics Laboratory, National Cheng Kung University, Tainan, Taiwan, ROC

[2] Assistant Researcher of Tainan Hydraulics Laboratory, National Cheng Kung University, Tainan, Taiwan, ROC

[3] Graduated Student of Hydraulic and Ocean Engineering Department, National Cheng Kung University, Tainan, Taiwan, ROC

breaking, air entrainment destroys the original flow structure, resulting in dissipation of wave energy. With the admixing of air bubbles, the flow fields of broken wave are turbulent and complicated. Although the energy dissipation and air bubbles mixing after wave breaking have been extensively studied in the past thirty years, its mechanism is not fully understood, due to the complex flow fields are essentially beyond the capacity of measuring equipments during that period. From theoretical and experimental studies, Horikawa and Kuo (1966) obtained an exponential decay function of wave height inside surf zone. Führböter (1970) assumed that the wave breaking provided the total dissipation energy to the air bubbles entraining into the water body, and derived the decay functions of wave height for spilling and plunging breakers respectively. Jansen (1986) employed the flow visualization technique and photochromism method to observe the turbulent flow fields of aerated layer in the outer region of surf zone. Recently, Nadaoka (1986) detected the turbulent intensity distributions in the nearshore zone by LDV. In the previous efforts, the connections of air bubbles entrainment with the turbulent energy dissipation had not been fully investigated. In order to understand this relationship, a special technique of He–Ne laser was employed to detect the entrainment process of air bubbles, and a LDV system was used to examine the spatial distributions of two dimensional velocity in wave flume respectively.

Experiments

It is very difficult to observe the kinematic phenomenon of air bubbles merged in water body. A special installation of He–Ne laser was developed, as depicted in Fig. 1. According to our experience, the transformed voltage signal from the He–Ne laser appears a drop-out when the laser beam is deflected by air bubbles. Such a phenomenon can be used to represent the variations of air bubbles. However, an appropriate threshold of background air concentration obtained in still water has to be determined before the data analysis process. A typical example is shown in Fig. 2 in which both the dash and solid line respectively denote the threshold value and drop-out signal. Furthermore, Lin & Hwung (1992) found out that the broken wave was a three dimensional flow field. Under this circumstance, air bubbles across the test section at the same phase of wave motion can't be identified by the laser beam. It is because that only the first bubble deflects the beam and the rest are hidden in the drop-out signal. Based on this conclusion, to determine a proper test width is very important in this experiment. From the results of total air concentration (C_t) with different test widths, as shown in Fig. 3a, it is obvious that a wider one possesses a higher concentration

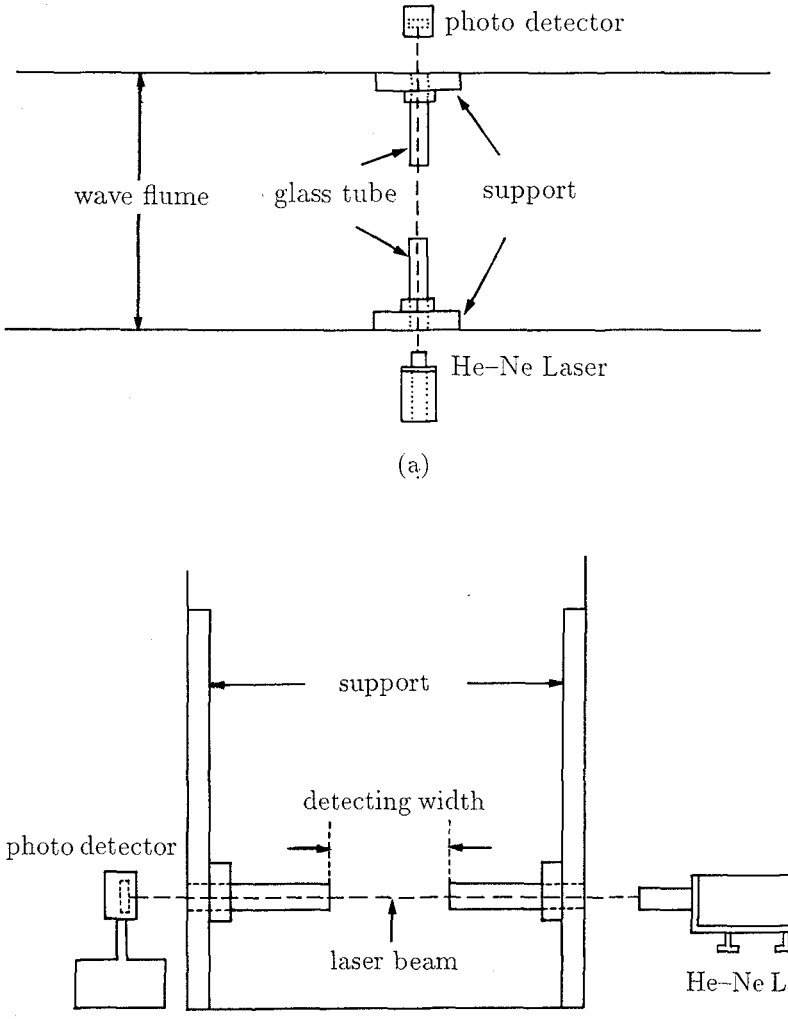

Figure 1. Experimental installation of air bubbles measurements; (a) top view, (b) front view

which doesn't linearly increase with the test width. When they are expressed in air concentration per unit width (C_u), as seen in Fig. 3b, the results of both of 3 and 4 cm test width are almost consistent, so that we adopt these two test widths for all of the experiments. In addition to the measurements

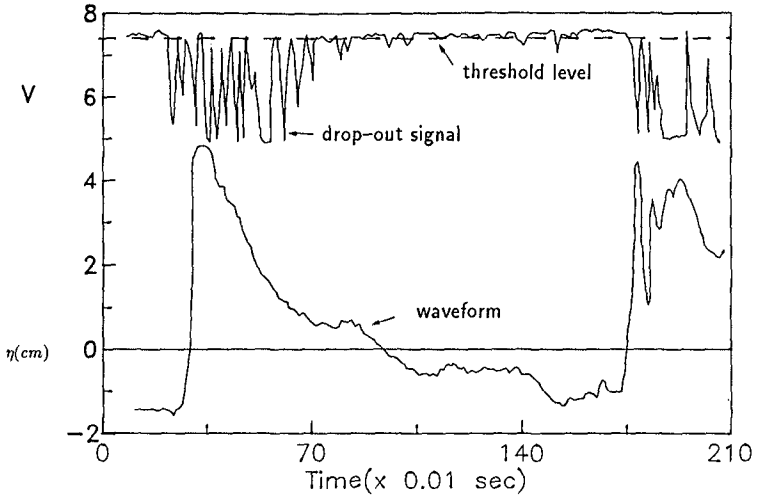

Figure 2. Drop-out signal induced by entrained air bubbles

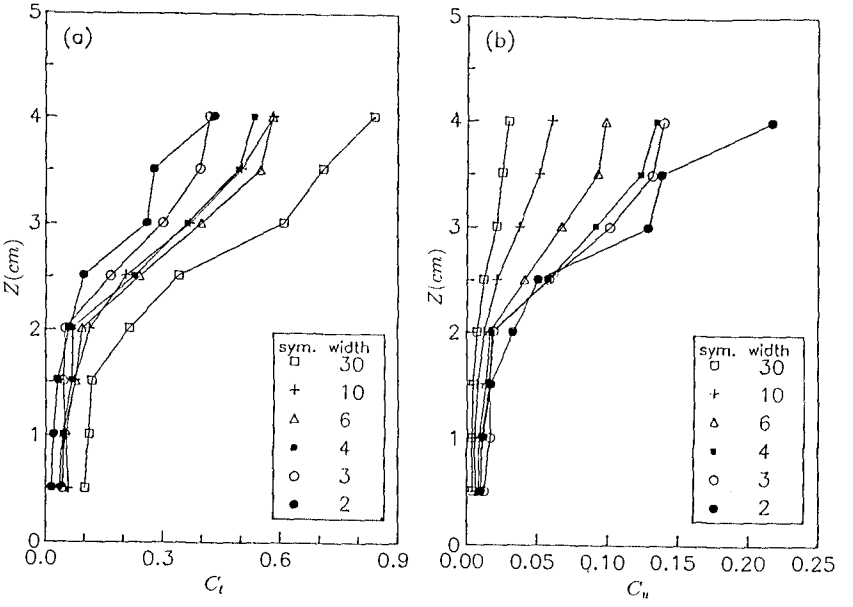

Figure 3. Concentration profiles of various test width; (a) total air bubbles concentration (C_t), (b) air bubbles concentration per unit width (C_u)

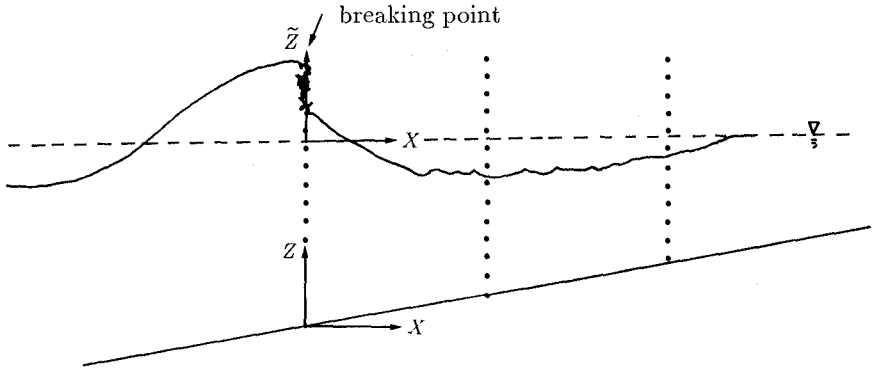

Figure 4. Schematic description of coordinate system and measuring points

Table 1. Experimental conditions

Case	T (sec)	h_i (cm)	H_i (cm)	Breaking type	H_b (cm)	H_o/L_o	h_b (cm)	H_b/h_b
1	1.29	33.0	6.11	plunging	8.08	0.0259	8.10	0.998
2	0.90	33.0	5.72	spilling	6.57	0.0483	7.00	0.925

of bubbles concentration, the turbulent flow fields in the surf zone was also detected by LDV (TSI—9100-8) of being capable to determine the variations of two dimensional velocity.

Two typical wave breaking were generated in the wave flume and the experimental conditions are tabulated in Table 1; in which T is the wave period in seconds, h_i the water depth at the horizontal portion of the flume, H_i the wave height produced by the wave generator, H_b the breaking wave height, H_o/L_o the converted wave steepness at deep water, h_b the water depth at breaking point, and finally H_b/h_b the relative water depth at the point of wave breaking. The bed slope of wave flume is 1/15. Fig. 4 shows the coordinate system and the distribution of measuring points. The first test section was positioned at the wave breaking point and the distances between measuring points in X and Z directions were 7.5 cm and 0.5 cm respectively.

Results and discussion

From the elaborate measurements, the vertical distributions of the concentration of entrained air bubbles for the plunging and spilling breakers are plotted in Fig. 5 and Fig. 6, respectively, in which L_o denotes the wave length in deep water. The concentration of air bubbles hyperbolically decreases with the water depth for both of the plunging and spilling breakers. As shown by Lin & Hwung (1992), the formation of water tongue by the plunging breaker, which violently impinges the water body, enhances the entrainment process of air bubbles. The maximum concentration of it, 18%, is larger than that of a spilling breaker, 12 %. The plunging breaker also induces a deeper penetration of air bubbles and a higher concentration within the aerated layer. When normalized by appropriate parameter groups, there exits a similarity function for different profiles and cases, which is shown in Fig. 7 and can be written as;

$$\frac{C}{C_o} = 0.56\left[\tanh\left(5.36\frac{Z_a}{\eta^+ + h_a} - 1.56\right) + 1\right] \tag{1}$$

where C is the air bubble concentration per unit width, C_o the air bubble concentration at still water level, η^+ the water surface elevation above the still water level. h_a denotes the penetration depth of air bubble based on the location where the duration of drop-out signal is 10 % of total sampling period. Z_a is the distance from the origin located at the penetration depth of h_a, and it is positive upward.

The longitudinal distributions of air concentration averaged on the aerated layer for cases of plunging and spilling breakers decrease with the dimensionless distance (X/L_o), as shown in Fig. 8. By the comparison with Kuo (1972), it shows that the theoretical prediction coincides with the experimental results of spilling breaker. However, it has much differences between the theoretical and experimental results due to the nonlinearity and strong impingement of plunging breaker. From a non-dimensionalized process, the cross-sectional average of air concentration shows a characteristic of similarity in Fig. 9. The similarity function can be expressed as;

$$\frac{\overline{C} - \overline{C}_{ha.max}}{\overline{C}_{imp} - \overline{C}_{ha.max}} = 2.85\exp(-1.72X/L_o) - 0.72 \tag{2}$$

where $\overline{C}$ represents the averaged concentration within the aerated layer, $\overline{C}_{imp}$ the averaged concentration at the impinging point of breaking wave,

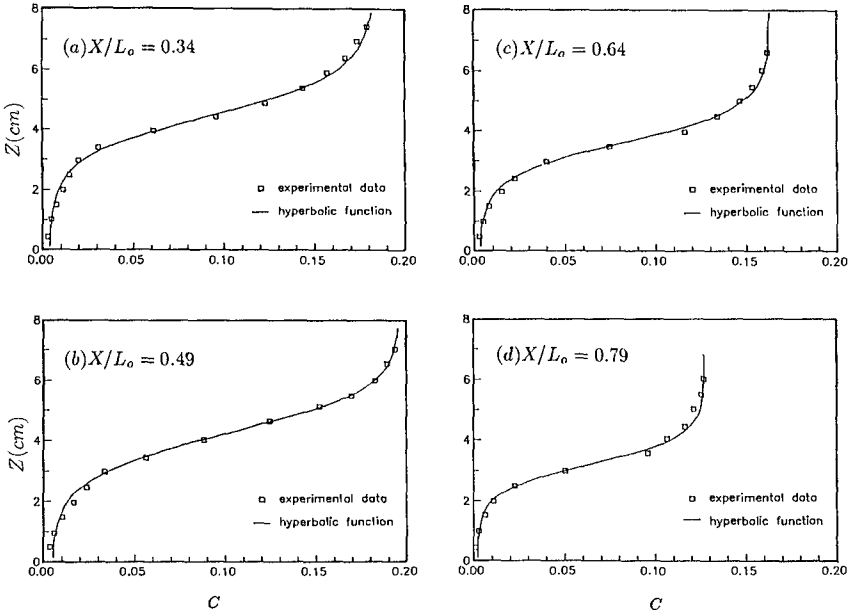

Figure 5. Vertical distribution of air bubble concentration (plunging breaker)

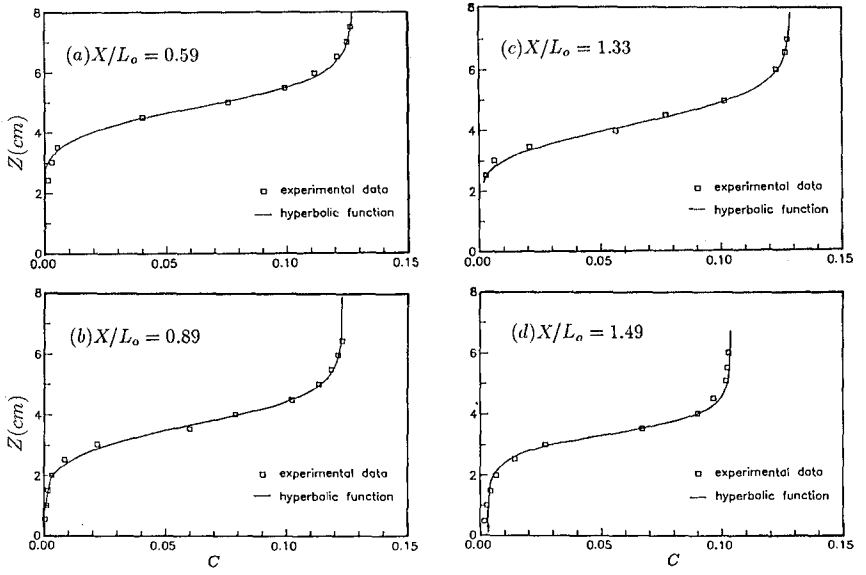

Figure 6. Vertical distribution of air bubble concentration (spilling breaker)

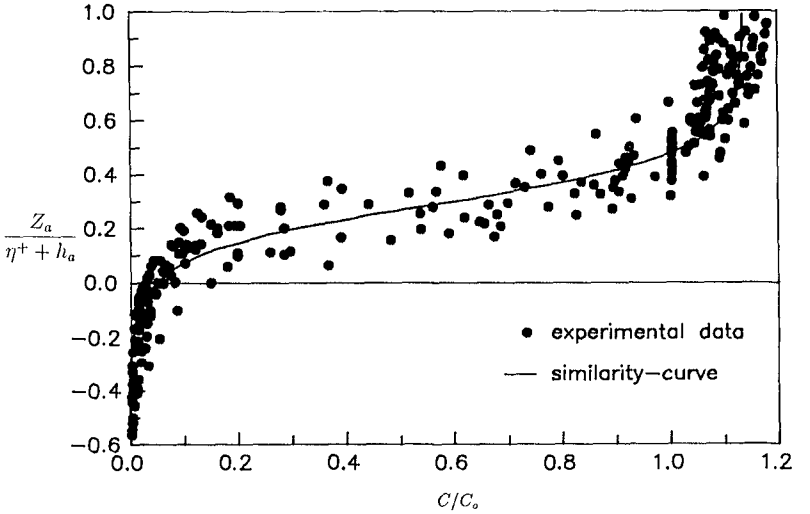

Figure 7. Similarity of vertical distribution of air bubble concentration

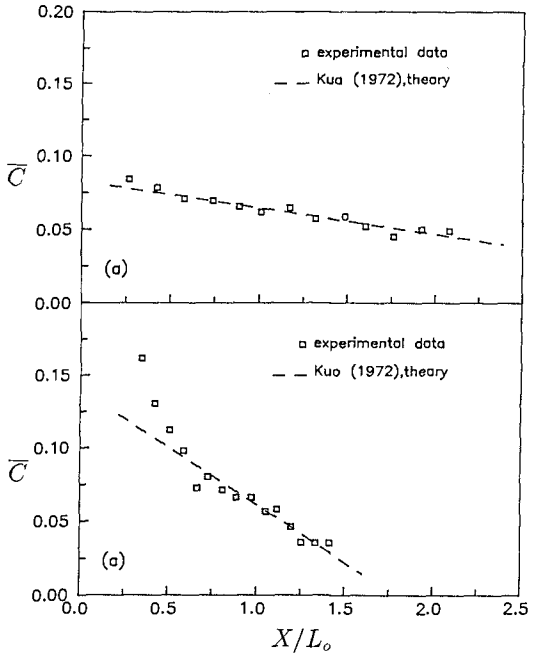

Figure 8. Average concentration along the longitudinal direction; (a) spilling breaker, (b) pluging breaker

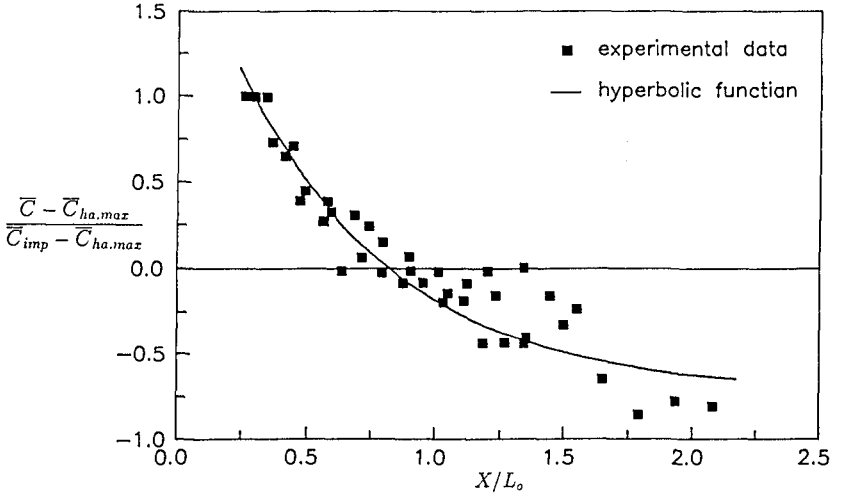

Figure 9. Similarity of cross-sectional averaged concentration of air bubbles

$\overline{C}_{ha.max}$ the averaged concentration at the maximum penetration section of air bubbles.

In order to understand the effect of air entrainment process on the turbulent flow fields after wave breaking, LDV was also employed to measure both of the horizontal velocity (u) and vertical velocity (w). According to IFFT (inverse fast Fourier transformation) method proposed by Hwung et al.(1989), the spatial distributions of air concentration, turbulent velocity intensities ($\sqrt{\overline{u'^2}}$, $\sqrt{\overline{w'^2}}$) and Reynolds stress ($-\overline{u'w'}$) are shown in Fig. 10 and Fig. 11 for cases of plunging and spilling breakers. It is obvious that the maximum of turbulent velocity intensities locate at the maximum penetration of air bubbles and so does the Reynolds stress. However, the positions of the maxima of velocity and its turbulent intensity don't coincide with each other. The former reaches the peak value in the impinging point. It is because that, when the wave breaking, there forms a water jet mixed with air bubbles impinging and penetrating into a deeper water depth. In the maximum of penetration section, the air bubbles begin to ascend due to the buoyancy effects and generate well-correlated velocity fluctuations. It enhances the energy transfer between different dimensions and results in the maximum of turbulent velocity intensities and Reynolds stress.

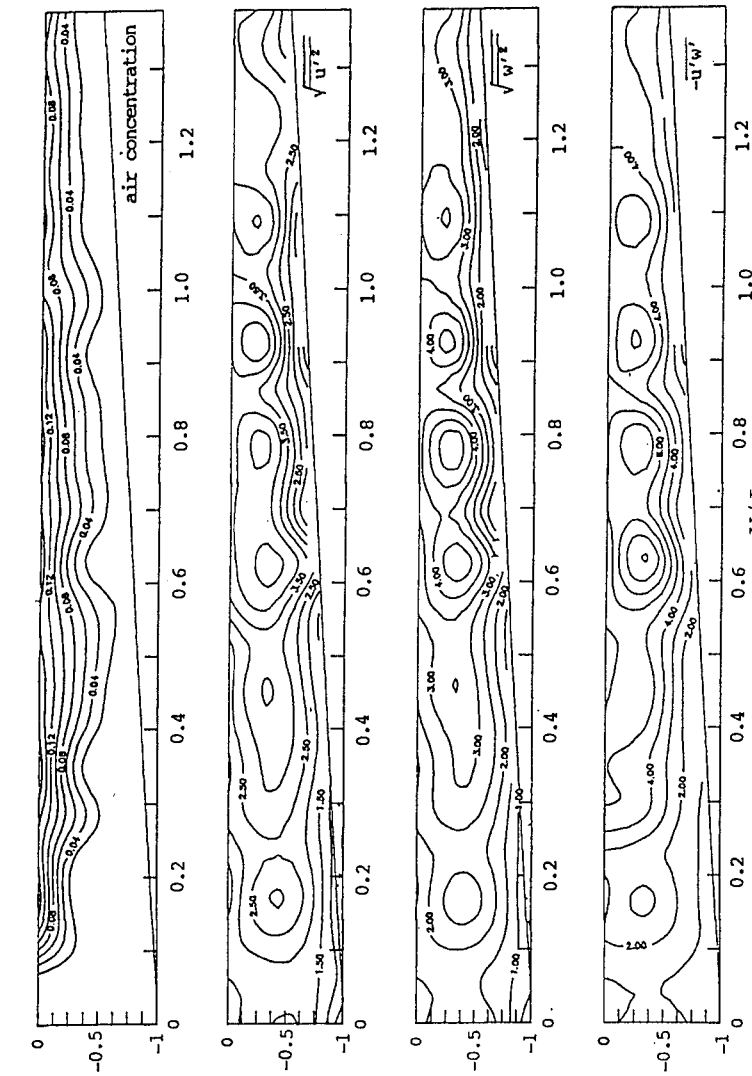

Figure 10. Spatial distribution of air concentration, turbulent velocity intensities and Reynolds stress (plunging breaker)

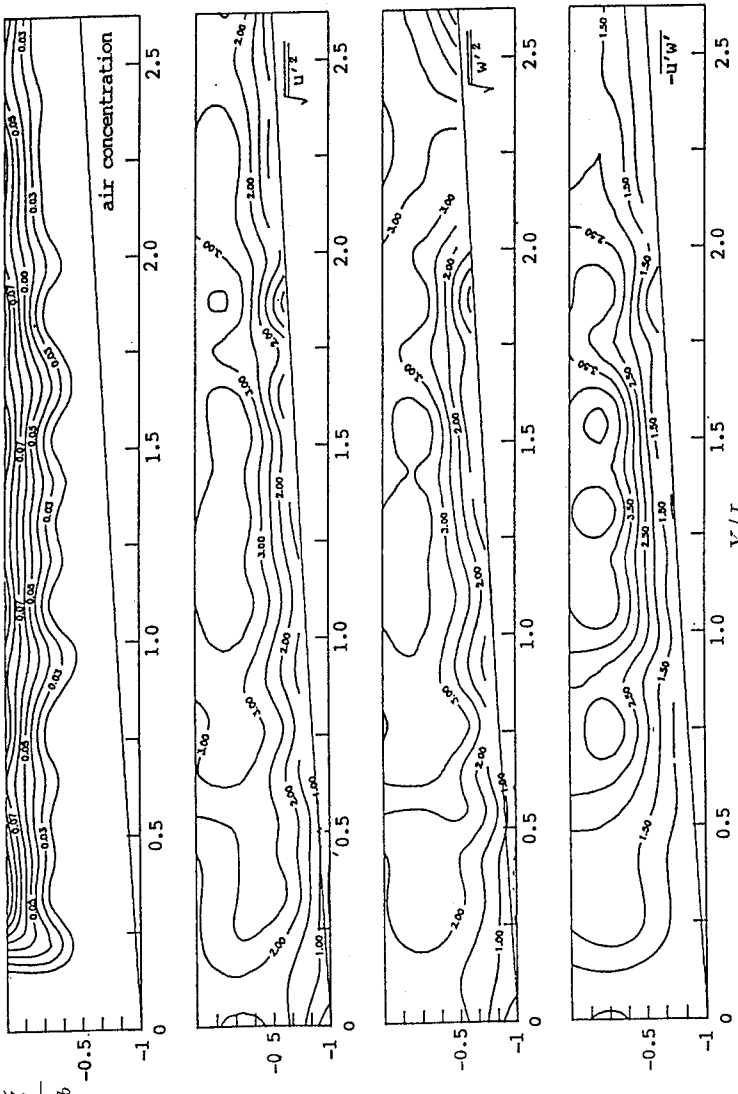

Figure 11. Spatial distribution of air concentration, turbulent velocity intensities and Reynolds stress (spilling breaker)

According to Führböter (1970), the potential energy of air bubbles inside surf zone can be expressed by;

$$E_{air} = \gamma \frac{{h_a}^2(x)}{2} \frac{\overline{C}}{1-\overline{C}} \tag{3}$$

where γ is the specific weight of water. In addition to the energy of air bubbles, the potential and kinematic energy (E_p, E_k) of the broken wave can be written as;

$$E_p = \frac{\gamma}{2} \frac{1}{T} \int_0^T \eta^2 dt \tag{4}$$

$$E_k = \frac{\rho}{2} \int_0^{h+\eta} \left[\frac{1}{T} \int_0^T (u^2 + w^2)\, dt \right] dz \tag{5}$$

where T and η are the sampling duration and the variations of water surface, respectively, while ρ denotes the water density. From Eq. (3) $\sim$ Eq. (5), the relationships between the energy of air bubbles and that of the turbulent flow fields for both of plunging and spilling breakers are plotted in Fig. 12 where the experimental results are non-dimensionalized by the total energy (E_b) at the breaking point of wave motion and E represents the summation of E_p and E_k. By the comparisons of experimental results, it shows that the variations of energy transfer can be divided into three stages in characteristics. The energy rapidly decreases before the impinging point of broken waves. Between the impinging point and the maximum penetration, the energy loss of the flow fields has been almost transferred into the potential energy of air bubbles since the summation of E_{air} and E nearly conserves. The kinematic energy slightly increases in the same region. Due to the buoyancy, the air bubbles ascend and induce the turbulence. The total energy of $E + E_{air}$ gradually decays in the rest region. The decaying tendency for the plunging breaker is faster than that of the spilling breaker since the entrainment of air bubbles is weaker for the spilling breaker.

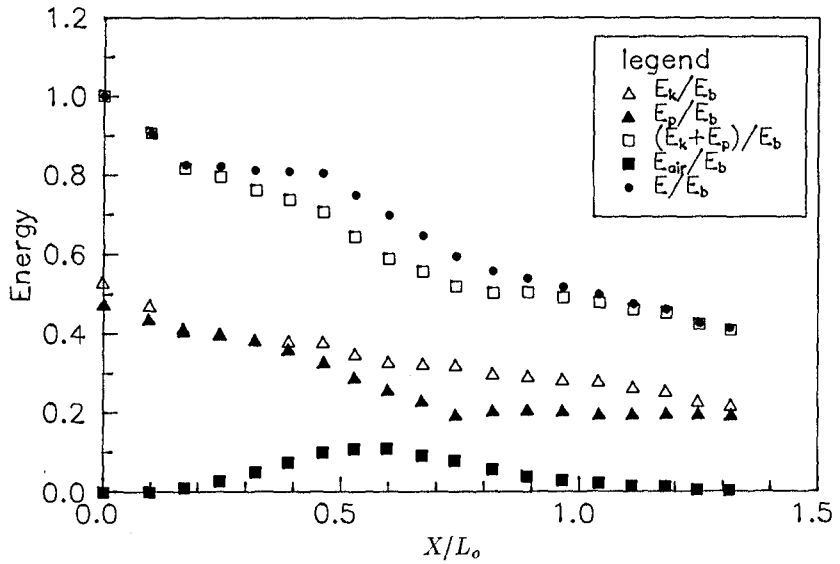

(a)

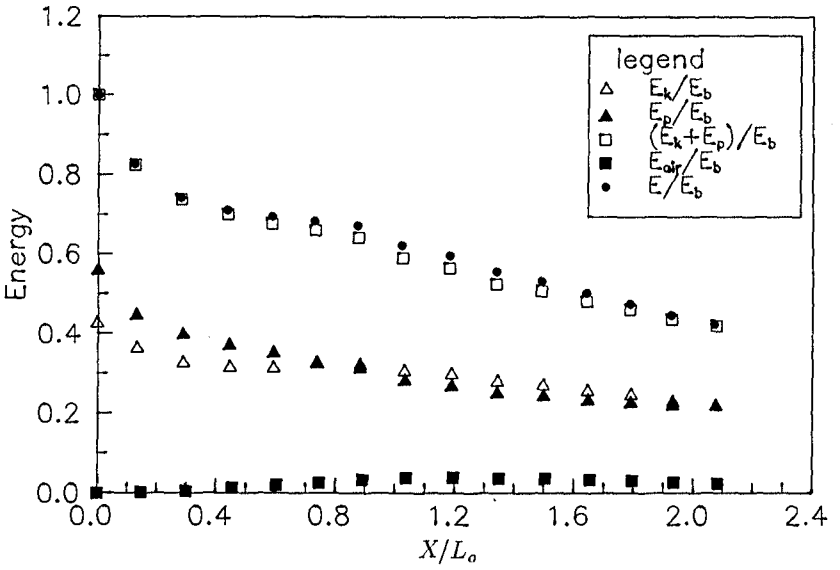

(b)

Figure 12. Variations of air bubbles energy, potential energy and kinematic energy ; (a) plunging breaker,(b) spilling breaker

Conclusion

According to the present study, the most important step in measuring air bubbles is to determine the significant width of detecting section which is 3~4 cm in our experiments. From the experimental results, the profiles of averaged air bubbles concentration decay hyperbolically and exponentially in the vertical and the horizontal directions. There exit similarity functions of air bubbles profiles if the experimental results are non-dimensionalized by appropriate parameter groups. For both of the plunging and spilling breakers, the turbulent velocity intensities and the Reynolds stress reach their maximum at the maximum penetration. The total energy shows multi-stages variations of rapid decrease, conservation and gradual decay in the region divided by the impinging point and the maximum penetration. The energy required for the air bubbles to merge into the water body is almost provided by the potential and kinematic energy.

Reference

1. Führböter, A.(1970), Air entrainment and energy dissipation in breakers, Proc. 12th Conf. on Coastal Eng., pp.391–398.

2. Jansen, P. C. M.(1986), Laboratory observations of the kinematics in the aerated region of breaking waves, Coastal Eng., Vol. 9, pp.453–477.

3. Horikawa, K. & Kuo, C. T.(1966),A study on wave transformation inside surf zone, Proc. 14th Conf. on Coastal Eng., pp.217–233.

4. Hwung, H. H., Lin, C. & Chyan, J. M.(1989), The characteristics of spectrum and velocity decomposition of the bottom flow in the surf zone, 13th Conf. on Theor. & Appl. Mech., Taichung, Taiwan, ROC, pp.1309–1320 (in chinese).

5. Kuo, S. T.(1972),The wave characteristics inside surf zone, Master these, National Cheng Kung University, ROC (in chinese).

6. Lin, C. & Hwung, H. H.(1992), External and internal flow fields of plunging breakers, Experiments in Fluids, Vol. 12, pp.229–237.

7. Nadaoka, K.(1986), A fundamental study on shoaling and velocity field structure of water waves in the nearshore zone, Technique Report, No. 36, Department of Civil Eng., Tokyo Institute of Technology, pp.33-125.